AIAA JOURNAL
Vol. 35, No. 9, September 1997

Technical Notes

TECHNICAL NOTES are short manuscripts describing new developments or important results of a preliminary nature. These Notes cannot exceed 6 manuscript pages and 3 figures; a page of text may be substituted for a figure and vice versa. After informal review by the editors, they may be published within a few months of the date of receipt. Style requirements are the same as for regular contributions (see inside back cover).

Numerical Solution of the Full Potential Equation Using a Chimera Grid Approach

Terry L. Holst*
NASA Ames Research Center, Moffett Field, California 94035

Introduction

THE purpose of this Note is to present results from a new algorithm for solving the full potential equation based on a chimera grid approach. The long term objective of this work is to develop a chimera-based full potential flow solver that will be compatible with the well-established OVERFLOW Euler/Navier–Stokes flow solver.[1–3] Thus, the user will have an option of which flow solver to use in the chimera-based zonal grid approach: full potential, Euler, or Navier–Stokes. Of course, the full potential option will not be applicable for all applications, but for those applications where the full potential equation is valid, the execution time should be up to two orders of magnitude less than for the Navier–Stokes formulation. Indeed, a chimera-based full potential solver should have modest execution times on even moderate-speed workstations. In a parametric study, the bulk of the required computations could utilize the full potential approach and then a few selected conditions could be checked with a more complete, and thus more accurate, Euler or Navier–Stokes simulation. Such an approach would be extremely cost effective especially considering that all of these approaches would utilize the same problem setup and postprocessing software and to a large extent the same grid generation software.

For most chimera zonal grid applications, there is not much information on error analysis. The questions of how much error the interpolation process produces and what the effect is of this error on various aspects of the solution away from the interface boundary have not been generally addressed. One notable exception to this is the work of Meakin,[4] in which a chimera scheme error analysis was performed for a number of steady and unsteady transonic airfoil cases. Results from this study demonstrated the viability of the chimera approach for the Euler formulation being used. The purpose of the present study is to investigate the prior two questions in the context of a chimera full potential solver.

Numerical Results

The steady, two-dimensional, full potential equation written in strong conservation-law form is solved in the present study using the Approximate Factorization, Scheme 2 (AF2), iteration scheme. Chimera boundary conditions at zonal grid interfaces are implemented using bilinear interpolation. This is the same type of interpolation interface employed in typical Euler or Navier–Stokes formulations utilizing the chimera approach. That is, both approaches utilize bilinear interpolation (trilinear in three spatial dimensions) on the scheme's dependent variables. For the present full potential formulation, the velocity potential is used, and typically for the Euler/Navier–Stokes approach, the standard conserved variables in the $\boldsymbol{Q}$ vector are used. Details of the present approach are given in Ref. 5 and will not be discussed further.

To evaluate the attributes of the chimera approach for solving the full potential equation, the flow over a two-dimensional circular cylinder is chosen. The simplicity of this problem allows comparisons between both numerical and analytical solutions and between various numerical solutions computed on both single-zone and multiple-zone chimera grids. In this study, both incompressible and shocked compressible cases are considered. Because of the existence of an exact analytic solution for incompressible circular cylinder flow, error can be precisely computed and used to determine detailed characteristics of the present chimera approach.

A schematic of the two-zone chimera grid arrangement used in this study to solve for the flow about a two-dimensional circular cylinder is displayed in Fig. 1. The outer grid is Cartesian, and the inner grid is polar. Key parameters for this grid arrangement are defined in Fig. 1. In addition to the two-zone chimera cases, single-grid flow computations using a simple polar-grid topology have also been computed for many of the cases studied herein. These single-zone grids are identical to the inner polar grid except that more points are added in the radial direction to allow the outer boundary position to approximately match that of the Cartesian grid in the corresponding two-zone case. Exact solution boundary conditions are used at the outer boundaries for both the chimera and single-grid approaches (incompressible flow only).

Pressure contours for the first result involving incompressible flow are displayed in Fig. 2. Contours are plotted for both grid zones, which creates two lines for each contour level in the chimera overlap region. Close examination of the pressure contours in the overlap region shows remarkable continuity, on both slope and position, with only small variations present.

Results from a grid refinement study are presented in Fig. 3. The grids utilized in this study range from 17×9 (Cartesian) and 17×7 (polar) to 257×129 (Cartesian) and 257×97 (polar). Each of the five grids utilized was carefully constructed so as to have the same outer boundaries, the same hole boundaries, and the same amount of spatial overlap at the chimera interface. Global rms error in the velocity potential plotted against grid spacing (Δ) is displayed in Fig. 3, where $\Delta = NI^{-1}$ and NI is the number of grid points on

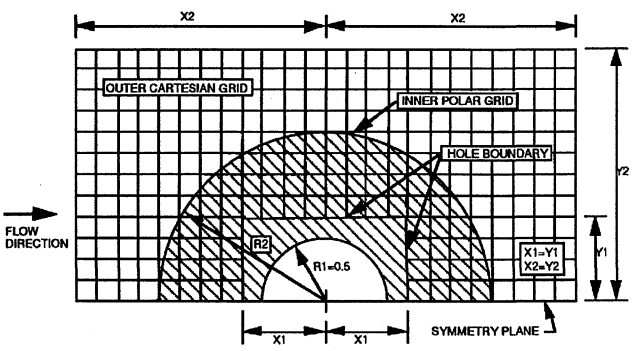

Fig. 1 Schematic of the two-zone chimera grid arrangement used in the present study to solve the flow over the upper half of a two-dimensional circular cylinder.

Received May 4, 1996; revision received April 21, 1997; accepted for publication April 21, 1997.

*Research Scientist, Advanced Computational Methods Branch. Fellow AIAA.

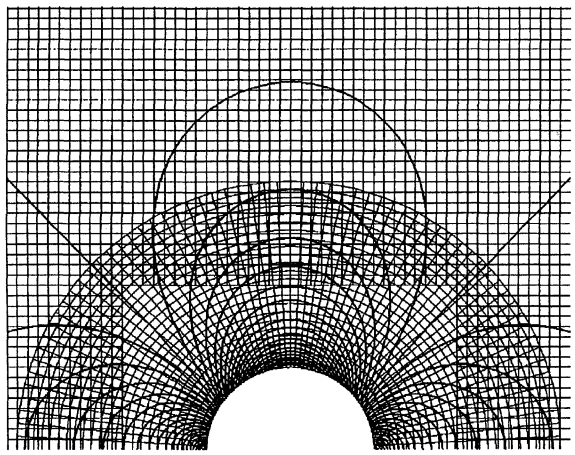

Fig. 2 Pressure contours surrounding the circular cylinder showing the inner polar grid solution, a portion of the outer Cartesian grid solution, and the region where the two solutions overlap, $M_\infty = 0.01$; two-zone grid: inner = 65 × 25, outer = 129 × 65, $R2 = 1.68$, $X1 = 1.0$, and $X2 = 4.0$.

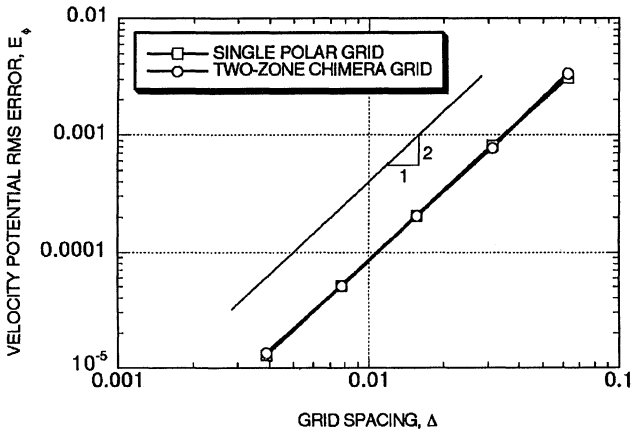

Fig. 3 Effect of grid refinement on the global rms error in the velocity potential, $M_\infty = 0$; single-zone grid: $R2 = 3.65$; two-zone grid: $R2 = 1.68$, $X1 = 1.0$, and $X2 = 4.0$.

the cylinder surface. Velocity potential values at all grid points, including all values in the chimera overlap region for the two-grid chimera cases, are used in computing this error. As can be seen from Fig. 3, the velocity potential error curves for both the two-grid chimera and single-grid approaches are almost identical. Both drop at the expected second-order rate.

The next case used to evaluate the chimera approach is a compressible flow case ($M_\infty = 0.5$) containing a strong shock wave. The geometry and general grid topology for the compressible cases are identical to the preceding incompressible cases. However, one change was to move the outer Cartesian grid hole boundaries as close to the circular cylinder as possible. This allows an evaluation of the chimera scheme as the shock wave passes through the inner interpolation boundary. The new hole boundary position allows a minimum clearance of two computational cells between the hole boundary and the circular cylinder geometry. The grid used for this case consists of a 129 × 49 inner polar grid and a 257 × 129 outer Cartesian grid. A small amount of grid stretching is employed to move the outer boundary to a position about 17 diameters away from the circular cylinder where freestream conditions are applied.

Mach number contours for the compressible computation are displayed in Fig. 4. The entire circular cylinder and inner interface boundary are displayed. The Mach number contours pass through the chimera interface boundary smoothly and without discontinuities in slope. Away from the shock and in the overlap region, contours from the inner and outer grids are nearly coincident. In the vicinity of the shock, it is evident that the coarseness associated with the outer grid relative to the inner grid (especially in the axial direction) causes a slight additional smearing in the shock wave at

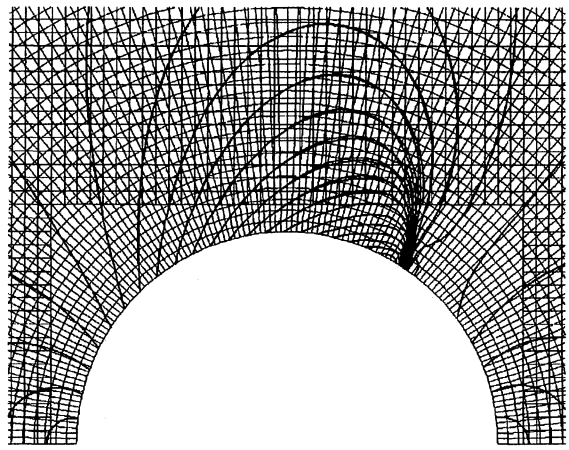

Fig. 4 Mach number contours surrounding the circular cylinder computed using the two-zone chimera grid. Details displayed include the entire surface solution and the entire inner chimera interface boundary, $M_\infty = 0.5$; inner grid = 129 × 49, outer grid = 257 × 129, $R2 = 2.46$, $X1 = 0.5625$, and $X2 = 17.5$.

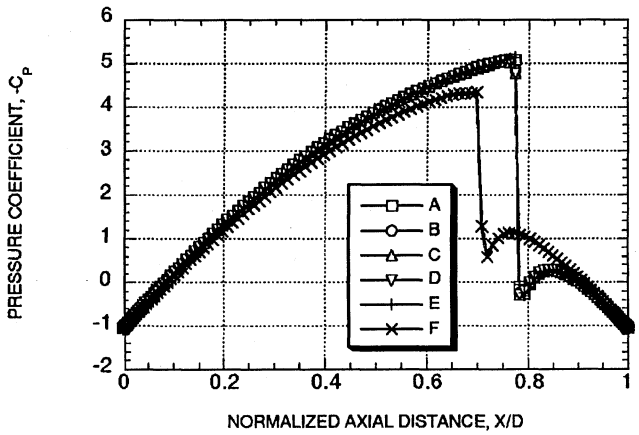

Fig. 5 Surface pressure coefficient distributions showing the effects of outer-zone grid refinement for the two-zone chimera grid arrangement, $M_\infty = 0.5$, $R2 = 2.46$, $X1 = 1.0$, and $X2 = 17.5$; inner grid = 129 × 49 (fixed); outer grid: A, 17 × 9; B, 33 × 17; C, 65 × 33; D, 129 × 65; E, 257 × 129; and F, no outer grid, freestream applied directly to inner-grid outer boundary.

the interface boundary. This is an expected behavior as the higher gradient associated with the shock wave cannot completely be supported on the coarser outer grid.

Next, it is of interest to study the effect of grid refinement when only the outer grid is refined. The shocked compressible solution is used for this study. In this series of cases the inner-grid dimensions are fixed at 129 × 49, and the outer-grid dimensions are varied from 17 × 9 to 257 × 129. Figure 5 shows a comparison of surface pressure computed using this sequence of grids. One additional curve corresponding to no outer grid is displayed, i.e., the inner grid of 129 × 49, with freestream boundary conditions imposed at its outer boundary, is used to produce this last curve (curve F). For this case, the outer boundary is located a little less than two diameters beyond the cylinder surface. As seen from Fig. 5, the outer-grid refinement level has only a small effect on the surface pressure, an amazingly small effect. All grids produce essentially the same result. And yet, if the outer grid is removed, the resulting surface pressure is dramatically in error. Thus, the outer grid serves a very important function, but its level of refinement (at least for the present case) is not important. One probable explanation for this behavior is that the present solution approaches freestream very rapidly away from the surface, and although the local solution is not that close to freestream, it is smooth enough to be reasonably captured on a coarse grid. The present solution, although a relatively benign case (transonic airfoil flows would be more difficult), does demonstrate flexibility for the present full potential chimera approach.

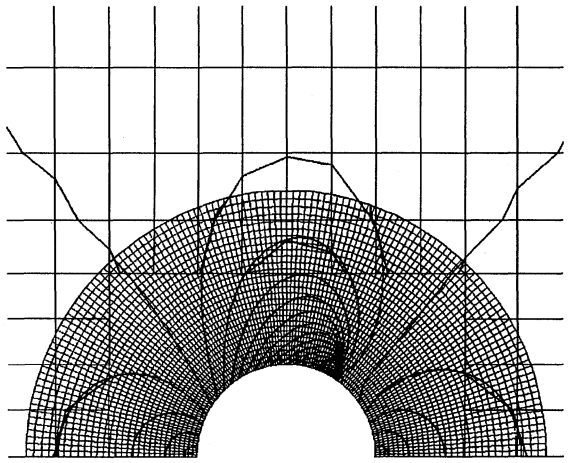

Fig. 6 Mach number contours surrounding the circular cylinder showing minimum chimera-grid overlap and coarse outer-grid conditions, $M_\infty = 0.5$, inner grid = 129 × 31, outer gird = 33 × 17, $R2 = 1.5$, $X1 = 1.0$, and $X2 = 17.5$.

A final solution demonstrating the effects of reduced chimera overlap and a coarse outer grid is displayed in Fig. 6. The inner- and outer-grid dimensions are 129 × 31 and 33 × 17, respectively. Note that the chimera overlap for this case has been significantly reduced. The large disparity in grid spacing at the inner-grid outer boundary is obvious. Nevertheless, the Mach number contours from the two grids in the overlap region are nearly identical to each other. The largest discrepancy in the overlap region arises from the straight-line segments used by the plotting program to represent the contours within each outer-zone grid cell. The solution at the circular cylinder surface, including the shock wave structure, is almost exactly the same as in Fig. 4. The surface pressure coefficient distribution for this case (not shown) is also in excellent agreement with similar results computed using different grid arrangements.

Concluding Remarks

A chimera-based full potential algorithm has been studied using a simple two-dimensional circular cylinder model problem. Both incompressible and shocked-compressible solutions have been used. The results indicate that the multizone chimera grid approach is a viable technique for solving the full potential equation and could provide a very fast computational tool for aerodynamic analysis and design.

A careful study of error produced by the chimera approach was conducted using a two-dimensional, incompressible model problem. A grid refinement study produced nearly identical results from single-zone and two-zone chimera grids, both exhibiting second-order behavior over a wide range of grid refinement. Thus, the additional interpolation-induced error generated by the chimera approach does not affect the basic second-order accuracy of the present numerical scheme.

Numerous chimera-grid arrangements with widely varying overlaps and cell-interface area ratios produced remarkable accuracy (and consistency in accuracy as well) showing little variation in the solutions being studied. In particular, remarkable accuracy at the circular cylinder surface was obtained using an extremely coarse outer grid in the chimera-grid arrangement. These results were produced with the shocked-compressible solution in which a transonic shock wave passed through one of the chimera interface boundaries.

References

[1]Steger, J. L., Dougherty, F. C., and Benek, J. A., "A Chimera Grid Scheme," *Advances in Grid Generation*, edited by K. Ghia and U. Ghia, ASME FED-5, American Society of Mechanical Engineers, New York, 1983, pp. 59–69.

[2]Benek, J. A., Buning, P. G., and Steger, J. L., "A 3-D Grid Embedding Technique," AIAA Paper 85-1523, July 1985.

[3]Buning, P. G., Chan, W. M., Renze, K. J., Sondak, D. L., Chiu, I. T., and Slotnick, J. P., "OVERFLOW User's Manual," Unpublished NASA Rept., Version 1.6ad, March 1993.

[4]Meakin, R., "On the Spatial and Temporal Accuracy of Overset Grid Methods for Moving Body Problems," AIAA Paper 94-1925, June 1994.

[5]Holst, T. L., "Numerical Solution of the Full Potential Equation Using a Chimera Grid Approach," NASA TM-110360, July 1995.

D. S. McRae
Associate Editor

Study of Adaptive Shape Airfoils at Low Reynolds Number in Oscillatory Flows

Wei Shyy,* David A. Jenkins,† and Richard W. Smith‡
University of Florida, Gainesville, Florida 32611

Introduction

MICROAERIAL vehicles (μAVs) with characteristic lengths under 6 in. (15 cm), flight speeds of 20–40 mph (32–64 km/h), and specific payload and endurance needs are potentially useful for many military and civilian applications. The combination of small dimensions and modest flight speed results in Reynolds numbers ranging between 10^4 and 10^5. Traditional rigid airfoil shapes experience substantial degradation in performance (specifically, the lift-to-drag ratio) as the Reynolds number falls through this range. Thus, even ordinary variations in wind speed can cause unwanted changes in behavior. In this study, rudimentary adaptive airfoils, which change their shape in response to changes in velocity, are examined for potential applications in this arena. Candidate designs are first evaluated by the application of detailed computational fluid dynamics simulations in a fluctuating flow. Then, several experimental airfoils are tested in a specially modified wind tunnel to look for corroboration of the predicted effects and other indications of potentially useful behavior.

Theoretical Formulation

A computational methodology has been developed to handle the fluid flow and flexible wing surface structure interaction in the context of a moving boundary problem.[1–3] In addition to solving a set of coupled, nonlinear partial differential equations governing the fluid and structural dynamics, detailed interfacial conditions must be prescribed at the solid–fluid interface at each instant in time. Furthermore, because the location of the solid–fluid interface is not known a priori, the interface position must be computed as part of the overall solution. For this study, the membrane is assumed to be massless with zero thickness and no initial strain. It is considered to be fixed at the leading and trailing edges. The membrane material is assumed to be linearly elastic and in a state of uniaxial stress as it deforms under the aerodynamic loads. The flow is modeled using the Reynolds-averaged Navier–Stokes equations, representing the Reynolds stresses in terms of the mean flow strain rate and an eddy viscosity. The k–ω eddy-viscosity model by Menter[4] is used here.

In the numerical method used, a discrete form of the elastic boundary value problem is obtained at a finite number of points using appropriate second-order accurate finite volume approximations. A pressure-based sequential-implicit algorithm, as described by Shyy,[5] is adopted as the flow solver. The turbulence and membrane equilibrium equations are simply appended to the basic conservation law equation set. All computations are done using time-dependent

Received Dec. 28, 1996; revision received May 1, 1997; accepted for publication May 30, 1997.

*Professor and Chair, Department of Aerospace Engineering, Mechanics and Engineering Science. Associate Fellow AIAA.

†Associate Engineer, Department of Aerospace Engineering, Mechanics and Engineering Science.

‡Postdoctoral Fellow, Department of Aerospace Engineering, Mechanics and Engineering Science; currently Engineer, Naval Surface Weapon Center, Panama City, FL 32407.